Solid State Sciences 13 (2011) 1921–1925

Contents lists available at SciVerse ScienceDirect

Solid State Sciences

journal homepage: www.elsevier.com/locate/ssscie

Photoconductivity and photo-detecting properties of vacuum deposited ZnSe thin films

K. Gowrish Rao [a,*], Kasturi V. Bangera [b], G.K. Shivakumar [b]

[a] Department of Physics, Manipal Institute of Technology, Manipal University, Manipal, Udupi 576104, India
[b] Thin films Lab, Department of Physics, National Institute of Technology Karnataka, Surathkal, Mangalore 575025, India

ARTICLE INFO

Article history:
Received 4 June 2011
Received in revised form
24 July 2011
Accepted 11 August 2011
Available online 22 August 2011

ABSTRACT

The paper reports the detailed analysis of photoconductivity and photo-detecting properties of vacuum deposited zinc selenide (ZnSe) thin films. The vacuum deposited ZnSe films were found to have high absorption coefficient and showed peak photo-response at 460 nm. The photocurrent and photo-response time of the films were measured as a function of substrate temperature and annealing conditions. Considerable increase in photocurrent and much faster photo-response was observed in films deposited at high substrate temperatures. Annealing at moderate temperatures also improved the photoconductivity and response time of the films.

1. Introduction

Zinc selenide (ZnSe) is an II–VI semiconductor compound with a direct bandgap of 2.7 eV, which is optimum for absorption and emission in the blue region of the electromagnetic spectrum [1–6]. Hence it is being looked at as a potential candidate for the fabrication of optoelectronic devices in the visible region. However the earliest efforts to exploit the properties of ZnSe were severely impeded by the difficulties in doping the material [7]. This long standing problem was finally overcome in 1990s when successful p-type doping of ZnSe was reported [8,9]. This success has motivated intensive research on ZnSe.

Thin films of ZnSe material have been prepared by many methods including molecular beam epitaxy [9,10], MOVPE [11–13], pulsed laser deposition [14,15] and vacuum deposition [1,16,17]. Extensive studies have been done on crystalline ZnSe which in turn resulted in the fabrication of ZnSe based blue LEDs [18]. ZnSe based lasers have been already used for a prototype demonstration in high-density CD players [19].

Apart from LED, ZnSe has a great potential for photo-detector applications [20–22]. At present the photo-detectors used in the visible region are mainly based on silicon. The efficiency of silicon based devices is low in visible region because Si has an indirect bandgap in the infrared region [22]. On the other hand, the quantum efficiency of ZnSe based devices is expected to be high as it has a direct bandgap and high absorption coefficient. ZnSe based photo-diode with quantum efficiency of 8%, have been already reported [21]. If the properties of ZnSe are optimized, then they may even have a potential efficiency of 60%. While intensive research is being done on photoconductivity of ZnSe [23,24], they are mainly based on epitaxial films obtained by higher end methods such as MBE, MOVPE etc. There is an immediate need to focus on preparing device quality ZnSe films by low cost methods so as to make them commercially viable.

In the present research work the photoconductivity and photo-response properties of vacuum deposited ZnSe films have been investigated. The effects of substrate temperature and annealing process on the photo-response properties of the films have been analysed.

2. Experimental details

Thin films of ZnSe material used in the present work were prepared by vacuum deposition technique. The films were deposited on well cleaned borosilicate glass substrates in a 12 inch vacuum coating unit (HINDHIVAC 12A4D). High purity (99.99%) ZnSe ingots (Aldrich) were used as source material for the films. Molybdenum boat was used for evaporating the source material, by resistance heating, under a residual pressure of less than 10^{-5} torr. The deposition rate was set at 30 nm/min. A substrate heater with a temperature controller was used to heat the substrates to desired temperatures. For electrical and photoconductivity studies, silver electrical contacts were made on the ZnSe films by vacuum deposition. These silver contacts showed

* Corresponding author.
E-mail addresses: kgowrishrao@gmail.com, rgknitk@gmail.com (K. Gowrish Rao).

1293-2558/$ – see front matter © 2011 Elsevier Masson SAS. All rights reserved.
doi:10.1016/j.solidstatesciences.2011.08.017

ohmic behaviour. The films of thickness 500 nm were used in the present work.

In order to study the effects of annealing process, the films were annealed in a hot air oven at different temperatures for 4 h. The maximum annealing temperature used was 540 K. The films annealed at temperatures higher than 540 K developed small cracks due to thermal stress.

Before studying the photo-response properties of the films, a detailed study of their crystal structure and chemical composition was undertaken. The crystal structure of the films was studied with the help of a Rigaku Miniflex X-ray diffractometer (Cu target, operating at 30 kV). The composition of the films was analysed by energy dispersive spectroscopy (EDS) (JEOL JSM 5800). The value and nature of the bandgap of the films was determined by absorbance studies using a spectrophotometer (PI-Acton). The electrical conductivity of the films was measured by Hall effect analysis using Van-der-Paw method [25].

The schematic diagram of the ZnSe photo-detector is shown in Fig. 1. The photoconductivity and photo-response studies were carried out in a dark chamber at room temperature. The experimental setup comprised a 150 W Xenon arc lamp (Newport) light source and a computer controlled monochromator with a photomultiplier tube detector (PI-Acton). In order to study the photoconductivity of the films, the light from the Xe arc lamp was passed through the monochromator to get a beam of desired wavelength. This light beam was then allowed to fall on the film kept inside the dark chamber. A suitable dc bias (9 V) was applied on the films to setup photocurrent. The photocurrent was measured as a difference between the currents flowing through the circuit, containing the film, under dark and illuminated conditions. A Keithley multimeter (model 2002) was used for accurate measurements of the currents.

The studies on speed of photo-response of the films were carried out in the similar way as described above. However, in these studies, an optical chopper was placed in front of Xe lamp to obtain pulsating light. The pulsating incident light produced alternating rise and fall in the photocurrent which in turn produced a corresponding rise and fall in the voltage across a standard resistance connected in series with the film. This change in voltage across the resistance was recorded by a digital storage oscilloscope (HP 54603B).

3. Results and discussion

The XRD patterns revealed the polycrystalline nature of the films. The films deposited at different substrate temperatures, and also the annealed films, were found to have the same cubic zincblende structure with a (111) texture. This texture arises in vacuum evaporated ZnSe films as (111) is the close-packing direction of zincblende structure. Such texture has been reported by many other researchers in the past [1,17]. The grain size of the films was determined using Scherer formula.

$$D = \frac{k\lambda}{\beta\cos\theta} \tag{1}$$

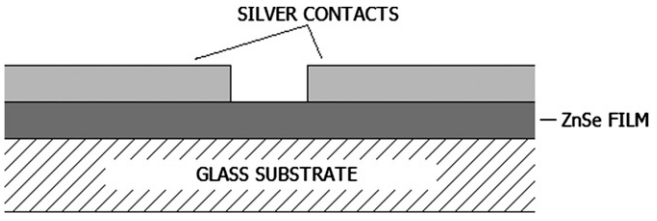

Fig. 1. The schematic diagram of ZnSe photo-detector (Not according to scale).

where k is the shape factor ($\sim$1), β is the full width at half maximum (FWHM) of the peak, θ is the Bragg's angle and λ is the wavelength of the X-rays used. The grain size of the films increased considerably with the increase in substrate temperature and also after annealing (Table 1).

The EDS analysis of the films revealed the dependence of the film composition on substrate temperature (Table 1). This is usually expected in thermally evaporated ZnSe films as the vapour pressures and sticking coefficients of zinc and selenium are different. The films deposited at room temperature were rich in selenium. The stoichiometric composition was achieved at a substrate temperature of about 423 K and the films deposited at temperatures above 423 K were rich in zinc. The electrical conductivity of selenium rich films, measured by Hall effect analysis, was found to be low and that of zinc rich films was comparatively higher (Table 1). The main reason for this is the self-compensation phenomenon which is very common in II–VI semiconductors. The excess selenium content in the films deposited below 423 K results in the spontaneous production of native defects which negate the acceptor-like action of selenium. As a result the films become more resistive. In the case of zinc rich films, the excess amount of zinc increases the n-type conductivity of the films. The post-deposition annealing of the films also changed the film composition due to the re-evaporation of excess selenium. The conductivity also increased accordingly. However, in the case of films which were deposited at substrate temperatures above 423 K, the conductivity decreased after annealing (Table 1). Since these films were already rich in zinc, annealing process only resulted in the re-evaporation of the excess amount of zinc. This fact was confirmed by the decrease in Zn:Se ratio of these films after annealing. Re-evaporation of zinc reduces the n-type conductivity of the films.

The absorption coefficient α of the films was found to be of the order of 10^4 cm^{-1}. Such high value of absorption coefficient is very much desirable for photo-detectors and solar cells. The absorption coefficient is in general related to frequency ν by the expression [26],

$$\alpha h\nu = B(h\nu - E_g)^n \tag{2}$$

where B is a constant and n takes the value 1/2, 2, etc. depending upon whether the transition is direct or indirect. A plot of $(\alpha h\,\nu)^m$ vs. $h\,\nu$ provides the information about the nature and value of the bandagap. The $(\alpha h\nu)^m$ vs. $h\nu$ curve drawn for a typical ZnSe film (Fig. 2), with $m = 2$, shows a linear region indicating that the bandgap of the film is direct. The value of the bandgap was obtained by extrapolating the linear region of the graph to meet the x-axis and it was found to be around 2.7 eV. The change in substrate

Table 1
The grain size, composition and electrical resistivity of ZnSe films as functions of substrate temperature and annealing conditions.

Substrate Temperature (K)	Annealing Conditions	Grain Size (Å)	Zn:Se	Resistivity (Ωcm)
300	Not Annealed	561	0.89	1113
373	Not Annealed	721	0.95	704
423	Not Annealed	813	1.00	512
473	Not Annealed	905	1.07	318
523	Not Annealed	1011	1.13	129
300	373 K, 4 h	612	0.91	732
300	473 K, 4 h	723	0.94	689
300	540 K, 4 h	804	0.98	594
373	540 K, 4 h	1053	0.99	576
423	540 K, 4 h	1136	1.05	498
473	540 K, 4 h	1221	1.03	503
523	540 K, 4 h	1336	1.01	523

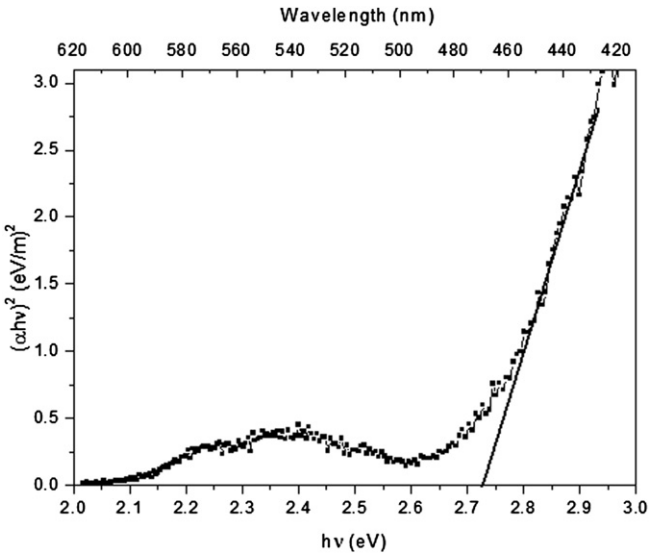

Fig. 2. The $(\alpha h\nu)^2$ vs. $h\nu$ curve of a typical ZnSe film.

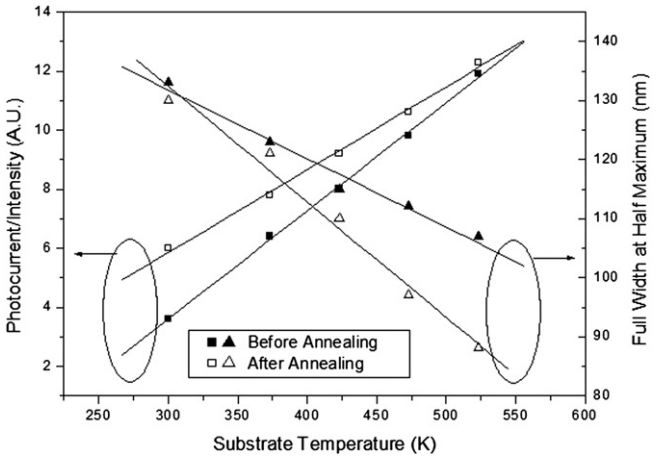

Fig. 4. The variation in peak value of photocurrent and width of the peak after annealing at 540 K for 4 h.

temperature and annealing process produced only marginal changes in the bandgap.

The spectral response curves of the ZnSe films, normalized with respect to the Xe emission spectrum, are shown in Fig. 3. The Fig. 3(a) represents films deposited at different substrate temperatures which are not subjected to annealing. The photocurrent is low in films deposited at room temperature. A considerable increase in the photocurrent was observed in films deposited at higher substrate temperatures. All curves show a peak at 460 nm which corresponds to the bandgap, 2.7 eV, of the films. This peak response at 460 nm indicates the possibility of using ZnSe in tandem solar cells for absorbing light in the shorter wavelength region of the solar spectrum. The photocurrent drops on either side of this peak wavelength. In the longer wavelength region, where obviously the inter-band transitions cannot take place, the transitions occur mainly from the shallow impurity levels. In the shorter wavelength region photocurrent decreases because the photons of these energies are absorbed at or near the surface of the semiconductor where the recombination is very high [27]. The increase in the photocurrent with substrate temperature can be explained by the model proposed by Slater [28] and Petritz [29]. According to this model, as the substrate temperature increases; the grain size of

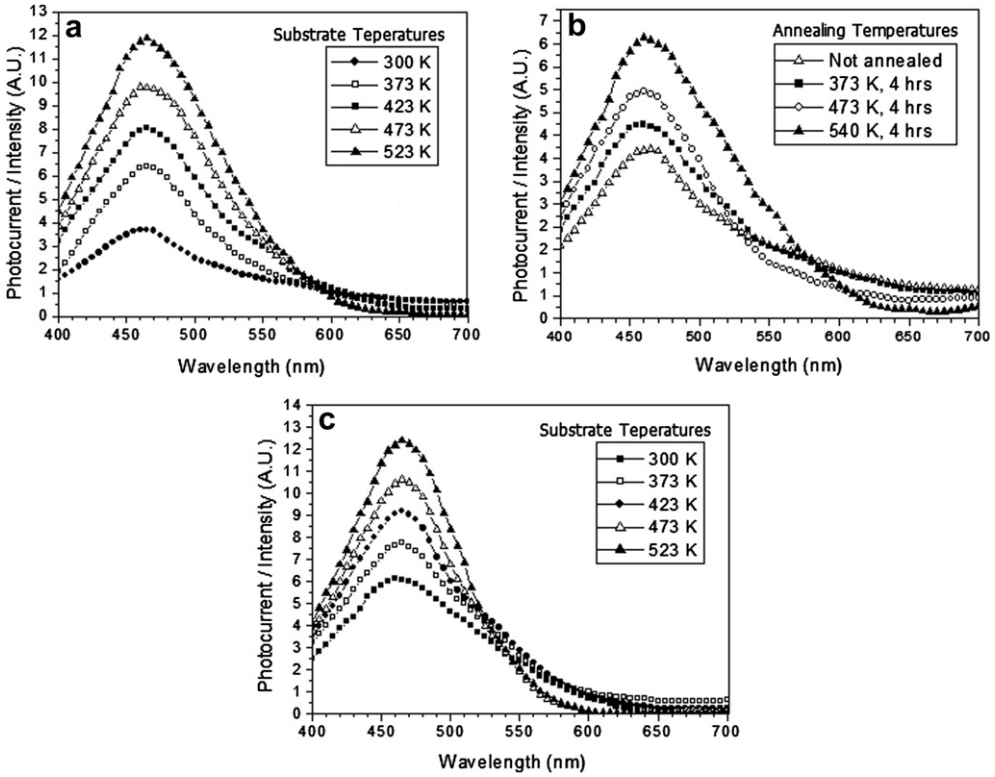

Fig. 3. The normalized spectral response curves of ZnSe films: (a) films deposited at different substrate temperatures but not annealed (b) Films deposited at 300 K and later annealed at different temperatures, (c) deposited at different substrate temperatures and later annealed at 540 K.

Table 2
The ratio of resistance of the films under dark (R_d) and illuminated (R_i) conditions as a function of substrate temperature and annealing conditions.

Substrate Temperature (K)	Annealing Conditions	R_d/R_i
300	Not Annealed	10.28
373	Not Annealed	25.58
423	Not Annealed	36.48
473	Not Annealed	49.40
523	Not Annealed	59.78
300	373 K, 4 h	21.05
300	473 K, 4 h	41.90
300	540 K, 4 h	49.25
373	540 K, 4 h	53.20
423	540 K, 4 h	68.78
473	540 K, 4 h	80.28
523	540 K, 4 h	88.03

Table 3
The rise and decay times of photocurrent as a function of substrate temperature and annealing conditions.

Substrate Temperature (K)	Annealing Conditions	Rise Time (μs)	Decay Time (μs)
300	Not Annealed	14	71
373	Not Annealed	12	47
423	Not Annealed	10	32
473	Not Annealed	8	25
523	Not Annealed	6	19
300	373 K, 4 h	13	53
300	473 K, 4 h	9	29
300	540 K, 4 h	6	20
373	540 K, 4 h	4	15
423	540 K, 4 h	3	12
473	540 K, 4 h	3	10
523	540 K, 4 h	3	9

the polycrystalline film increases, reducing the grain-boundary region. This in turn results in lowering of the inter-grain potential barrier. The inter-grain potential barrier further decreases upon illumination of the film. It can also be observed that the peak of the spectral response curve becomes sharper as the substrate temperature increases. This is due to the fact that the impurity concentration decreases with the increase in substrate temperature. The post-deposition annealing of the films also produced similar result (Fig. 3(b)). The combined effect of high substrate temperature and post-deposition annealing can be seen in Fig. 3(c). These curves have much sharper peaks due to the large decrease in the amount of impurities. The photocurrent also increased after annealing. However the increase in photocurrent, after annealing, is only marginal for films deposited above 423 K. This is due to the decrease in their n-type conductivity, resulting from the re-evaporation of zinc during the annealing process. The change in peak value of photocurrent and width of the peak, after the annealing process, are shown in Fig. 4. The width of the peak, in this case, is taken as the difference between two half maximum points.

The ratio of electrical resistance of the films under dark (R_d) and illuminated (R_i) conditions are given in Table 2. The illuminated resistance R_i was measured for the peak response wavelength of 460 nm. The large difference between R_d and R_i confirms the production of photo-generated carriers due to the influence of incident light. The ratio R_d/R_i increased with substrate temperature indicating the enhanced photoconductivity.

The speed of photo-response of the films was measured by observing the change in voltage across a standard resistance, resulting from pulsating light (460 nm) input. The pulse width of the incident light was chosen sufficiently large (around 1 ms) so as to allow the photocurrent to reach saturation. The oscilloscope images shown in Fig. 5 correspond to rise (Fig. 5(a)) and decay (Fig. 5(b)) of photocurrent. The time taken by the current to increase from 10% to 90% of the saturation value was taken as rise time and the time taken by the current to drop from 90% to 10% was taken as decay time. It can be seen that the rise in photocurrent is much faster than decay. The slowness of decay process is mainly due to the presence of impurities in the films which act as carrier traps. The traps hold the photo-induced charges for longer duration, prolonging the decay process. The rise and decay time decrease considerably with substrate temperature (Table 3). The elevated substrate temperature reduces the trap density in the films and hence both rise and decay processes become much faster. Since the annealing process also reduces the trap density, similar result was obtained in the case of annealed films.

The decay curve can be represented by the expression [30],

$$V(t) = V_0 e^{-pt} \tag{3}$$

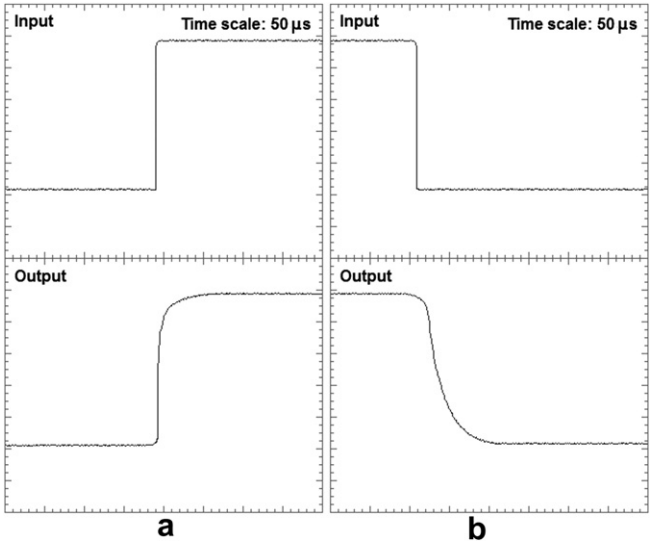

Fig. 5. The oscilloscope images (voltage-time curves) showing rise (a) and decay (b) of photocurrent in ZnSe films. The input is shown for reference.

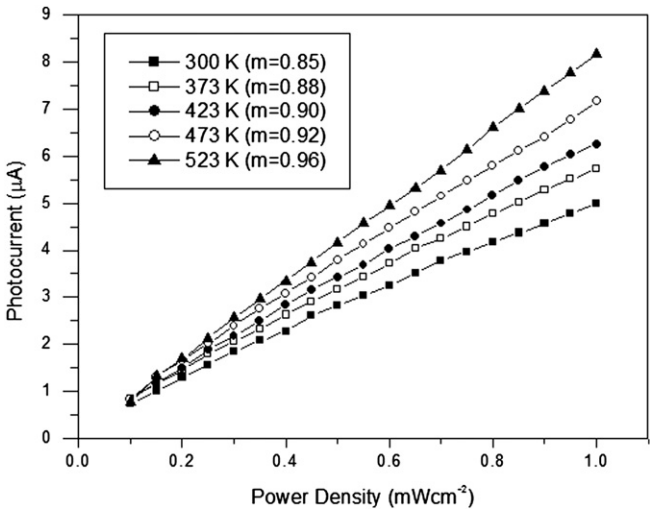

Fig. 6. The variation of photocurrent with power density of input light (460 nm), shown for ZnSe films deposited at different substrate temperatures.

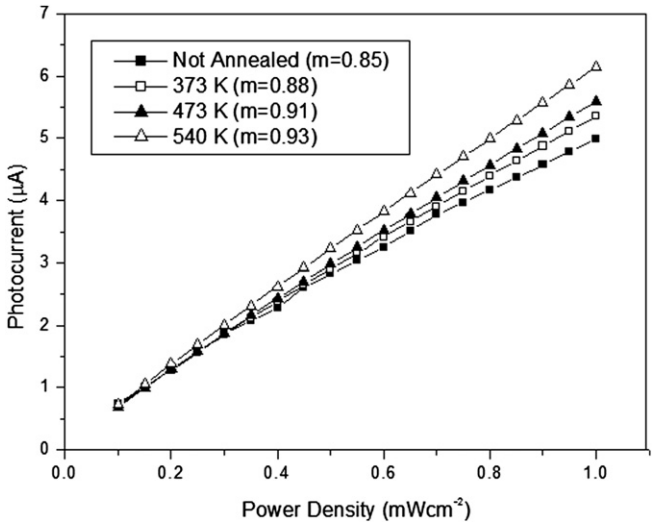

Fig. 7. The variation of photocurrent with power density of input light (460 nm) after annealing the ZnSe films at different temperatures for 4 h (Substrate Temperature: 300 K).

where $V(t)$ is the voltage at time t. The factor p is the probability of an electron escaping from trap per second and it is given by,

$$p = S\exp(-E_t/kT) \quad (4)$$

where $S = 10^{10}s^{-1}$ is the frequency factor and E_t is the trap depth. The trap depths measured for ZnSe films were in the range 0.1–0.18 eV.

The variation of photocurrent i_p with incident light power density p is shown in Fig. 6. Usually such variation follows the relation,

$$i_p \alpha p^m \quad (5)$$

where m is a number which can be equal to 1, less than 1 or greater than 1 corresponding to linear, sub-linear and super linear behaviours respectively. In the case of ZnSe films, the variation was found be slightly sub-linear. The value of m was found to be between 0.85 and 0.96. This sub-linear behaviour arises because of the exponential distribution of traps in the bandgap [27]. As the intensity of the radiation increases, the quasi-Fermi level shift towards the conduction band edge and an increasing number of traps are converted into recombination centres. As a result the photocurrent does not increase linearly with power density. However the value of m approaches unity for films deposited at higher temperatures, indicating that almost linear behaviour can be obtained at higher substrate temperatures. Post-deposition annealing also produced the same change (Fig. 7)

4. Conclusions

The photoconductivity and photo-detecting properties of vacuum deposited ZnSe films were studied as functions of substrate temperature and annealing conditions. The films were polycrystalline and were found to have a direct bandgap of 2.7 eV. They also had high absorption coefficient which is very useful for photovoltaic and photo-detector applications. The spectral response curves of the films showed a peak at 460 nm which matches very closely with their bandgap. Both the photoconductivity and the speed of photo-response of the films increase considerably with substrate temperature and post-deposition annealing owing to the decrease in inter-grain potential barrier and trap density. The variation of photocurrent with photo power density was found to be slightly sub-linear at low substrate temperatures. However it approaches linear behaviour as the substrate temperature increases.

References

[1] E. Bacaksiz, S. Aksu, I. Polat, S. Yilmaz, M. Altunbas, Journal of Alloys and Compounds 487 (2009) 280–285.
[2] C.D. Lokhande, P.S. Patil, A. Ennaoui, H. Tributsch, Applied Surface Science 123 (1998) 294–297.
[3] G.I. Rusu, V. Ciupina, M.E. Popa, G. Prodan, G.G. Rusu, C. Baban, Journal of Non-Crystalline Solids 352 (2006) 1525–1528.
[4] G. Riveros, H. Gómez, R. Henrýćquez, R. Schrebler, R.E. Marotti, E.A. Dalchiele, Solar Energy Materials and Solar Cells 70 (2001) 255–268.
[5] K.R. Murali, A. Austine, D.C. Trivedi, Materials Letters 59 (2005) 2621–2624.
[6] Chia-Wei Huang, Hsuan-Mei Weng, Yeu-Long Jiang, Herng-Yih Ueng, Thin Solid Films 517 (2009) 3667–3671.
[7] D.J. Chadi, Annual Review of Materials Science 24 (1994) 45–62.
[8] T. Marchall, D.A. Cammack, British Journal of Applied Physics 69 (1991) 4149.
[9] M.A. Haase, H. Cheng, J.M. Depydt, J.E. Pots, Journal of Applied Physics 67 (1990) 448.
[10] F. Nakanishi, H. Doi, T. Yamada, T. Matsuoka, S. Nishine, K. Matsumoto, T. Shirakawa, Applied Surface Science 117–118 (1997) 495–499.
[11] A.C. Wright, D. Gnoth, T.L. Ng, N. Maung, Applied Surface Science 123–124 (1 january 1998) 555–559.
[12] T. Yodo, T. Koyama, K. Yamashita, Journal of Crystal Growth 86 (1990) 273–278.
[13] F. Sakurai, K. Suto, Y. Oyama, J. Nishizawa, Journal of Crystal Growth 214–215 (2000) 537–541.
[14] J.L. Deiss, A. Chergui, L. Koutti, J.L. Loison, M. Robino, J.B. Grun, Applied Surface Science 86 (1995) 149–153.
[15] Z.P. Guan, G.H. Fan, S.H. Song, X.W. Fan, Thin Solid Films 217 (1992) 98–101.
[16] R. Pal, B. Maiti, S. Chaudhuri, A.K. Pal, Vacuum 46 (1995) 1255–1260.
[17] S. Venkatachalam, Y.L. Jeyachandran, P. Sureshkumar, A. Dhayalraj, D. Mangalaraj, Sa.K. Narayandass, S. Velumani, Materials Characterization 58 (2007) 794–799.
[18] M.A. Haase, J. Qiu, J.M. Depydt, H. Cheng, Journal of Applied Physics 59 (1991) 1272.
[19] K.W. Haberem, P.F. Baude, S.J. Flamholtz, M. Buijs, J.J. Horikx, K.K. Law, M.A. Haase, T.J. Miller, G.M. Haugen, Proceedings of SPIE The International Society for Optical Engineering 3001 (1997) 101.
[20] W. Fashinger, W. Spahn, J. Ntimbcrger, A. Gerhard, M. Kom, K. Schiill, D. Albert, H. Reis, R. R.EbelSchmit, B. Olszowi, M. Ehinger, G. Landwehr, Physica Status Solidi B. 202 (1997) 695.
[21] A. Gerhard, J. NUmberger, K. Schiill, V. Hock, C. Schumacher, M. Ehinger, W. Fashinger, Journal of Crystal Growth 184-185 (1998) 1319.
[22] U.V. Desnica, Progress in Crystal Growth and Characterization of Materials 36 (1998) 291–357.
[23] A. Bouhdada, M. Hanzaz, F. Vigué, J.P. Faurie, Applied Physics Letters 83 (2003) 171.
[24] C.W. Chang, H.C. Yang, C.H. Chen, H.J. Chang, Y.F. Chen, Journal of Applied Physics 89 (2001) 3725.
[25] L.J. Van der Pauw, Philips Technical Review. 20 (1958) 220.
[26] K.L. Chopra, S.R. Das, Thin Film Solar Cells. Plenum Press, 1983, 57–58.
[27] N.V. Joshi, Photoconductivity: Art, Science and Technology, vol. 95, Marcel Dekker Inc., 1990.
[28] J.C. Slater, Physical Review 103 (1956) 1631.
[29] R.L. Petritz, Physical Review 104 (1956) 1509.
[30] M. Buragohain, K. Barua, Thin Solid Films 99 (1983) L1.